American Mineralogist, Volume 81, pages 603–610, 1996

Mn crystal chemistry in pumpellyite: A resonant scattering powder diffraction Rietveld study using synchrotron radiation

G. Artioli,[1] A. Pavese,[1] M. Bellotto,[2] S.P. Collins,[3] and G. Lucchetti[4]

[1]Dipartimento di Scienze della Terra, Università di Milano, I-20133 Milan, Italy
[2]Institut Francais du Petrole, BP 311, F-92506 Rueil-Mailmaison, France
[3]Synchrotron Radiation Department, Daresbury Laboratory, Warrington WA4 4AD, U.K.
[4]Dipartimento di Scienze della Terra, Università di Genova, I-16132 Genoa, Italy

Abstract

The present study attempts to clarify the structural role of Mn in two pumpellyite specimens with the chemical formulas $Ca_{7.80}(Al_{8.91}Mn_{1.85}Mg_{1.16}Fe_{0.37})Si_{11.84}O_{56-x}OH_x$ and $Ca_{8.12}(Al_{7.99}Mn_{3.41}Mg_{0.71}Fe_{0.30})Si_{11.84}O_{56-x}OH_x$. The samples are from gabbroic breccias of the Bracco ophiolites (Eastern Ligurian Apennines, Italy), and their chemistry is typical of Mn-rich pumpellyite minerals associated with Mn mineralization in prehnite-pumpellyite metamorphic facies. The distribution of the Mn cations over the two crystallographically independent X and Y octahedral sites, and their prevalent oxidation states, were determined by Rietveld refinement from multiple powder data sets collected at different wavelengths for each sample using synchrotron X-rays. The powder data, collected in proximity to and far from the Mn*K* absorption edge, allowed refinement of the f' anomalous scattering parameter for each data set along with other variables during the Rietveld structure analysis, and we could thus estimate the oxidation state of Mn from the valence chemical shift of the absorption edge. The results indicate that Mn in pumpellyite is distributed over both octahedral sites, and the refined anomalous scattering coefficients clearly show that the two Mn valence states are segregated: Mn^{2+} is prevalent in the more symmetrical octahedral X site, and Mn^{3+} is prevalent in the octahedral Y site. The present results confirm the relationship between site partitioning and oxidation state of transition elements in pumpellyite that was previously proposed to explain the distribution of Fe cations in the structure.

Introduction

Pumpellyite, monoclinic space group $A2/m$, is generally regarded as a mixed-group silicate because both isolated SiO_4 tetrahedra and disilicate groups $[Si_2O_6(OH)]$ are present in its structure. The accepted classification scheme describing the chemistry of Al- and Fe-rich minerals sharing the pumpellyite-type structure (Passaglia and Gottardi 1973) essentially sets Al–end-member pumpellyite and Fe–end-member julgoldite as end-members of a solid-solution series encompassing Fe–end-member pumpellyite and Al–end-member julgoldite minerals. Cr–end-member-pumpellyite (shuiskite: Ivanov et al. 1981), Mn–end-member pumpellyite (okhotskite: Togari and Akasaka 1987), and V–end-member pumpellyite (Pan and Fleet 1992) should also be considered as structural analog end-members of the same group. Specifically, because pumpellyite from low-grade metamorphic rocks often contains a substantial amount of Mn, pumpellyite is better described in the Al-end-member pumpellyite–Fe-end-member julgoldite–Mn-end-member okhotskite compositional projection (Dasgupta et al. 1991).

The general chemical formula of the pumpellyite-group minerals is commonly written $W_8X_4Y_8Z_{12}O_{56-n}(OH)_n$, where W is a sevenfold-coordinated site primarily occupied by Ca, X and Y are two crystallographically independent octahedral sites occupied by Mg, Al, and divalent and trivalent transition metals (i.e., Fe, Cr, Mn, and V), and Z is a tetrahedral site invariably occupied by Si. The mineral is named pumpellyite, julgoldite, okhotskite, or shuiskite depending on whether Al, Fe, Mn, or Cr is the prevailing cation in the Y octahedral site. A suffix should be added to denote the dominant cation in the X octahedral site (Passaglia and Gottardi 1973).

Most of the structural studies concerning pumpellyite-type minerals have been performed by single-crystal X-ray diffraction on Al-rich (Gottardi 1965; Galli and Alberti 1969; Allmann and Donnay 1971; Baur 1971; Artioli 1980; Yoshiasa and Matsumoto 1985) and Fe-rich end-members (Moore 1971; Allmann and Donnay 1973). Several recent studies have revised the crystal-chemical role of Fe in pumpellyite-type structures by means of X-ray powder Rietveld refinement, X-ray absorption spectroscopy, and Mössbauer spectroscopy (Artioli et al. 1991, 1995; Artioli and Geiger 1994). These combined experiments have shown that the Fe valence state in pumpellyite is mostly trivalent, and that Fe^{2+} and Fe^{3+} are distinct over the two crystallographically independent

0003–004X/96/0506–0603$05.00

Table 1. Electron probe microanalyses (oxide wt%) of the Mn-rich pumpellyite

	Sample SN1		Sample SN5	
	Range of 19 points	Mean	Range of 35 points	Mean
SiO_2	32.78–34.99	33.80	33.18–35.84	34.76
Al_2O_3	18.13–20.27	19.36	19.97–23.98	22.05
Fe_2O_3	0.71–2.14	1.13	0.73–2.43	1.42
MnO	9.93–12.92	11.50	4.63–8.50	6.37
MgO	0.71–1.83	1.35	1.40–2.77	2.27
CaO	21.09–22.12	21.62	20.42–21.86	21.35

octahedral sites, with Fe^{3+} located on the smaller and more distorted Y site, and Fe^{2+} located on the larger and more regular X site. The crystal-chemical behavior of the transition metals in pumpellyite is of importance in the thermodynamic modeling of the stability field of the mineral during metamorphic processes (Frey et al. 1991).

The present study aims to clarify whether the Mn cations in the pumpellyite structure are similarly partitioned over the octahedral sites.

Sample preparation and characterization

Two natural Mn-rich pumpellyite samples, labeled SN1 and SN5, were studied. Both samples are from reported occurrences of Mn-rich pumpellyite minerals in gabbroic monogenic breccias included in the ophiolitic complexes of the Passo del Bracco, Eastern Ligurian Apennines, Italy (Lucchetti 1983). The Mn results from primary enrichment in the sedimentary matrix of the breccia and from chemical diffusion and replacement of femic phases in the gabbro clasts. The pumpellyite minerals presumably grew during mineralogic reequilibration under conditions of prehnite-pumpellyite facies metamorphism (Cortesogno et al. 1984). The thermobaric conditions are comparable to those reported for the occurrence of Mn-rich pumpellyite from Japan (Kato et al. 1981). Pumpellyite in these rocks is reported to be intimately associated with prehnite, albite, chlorite, quartz, and hematite (Lucchetti 1983). In the selected specimens, major mineral impurities detected by preliminary X-ray powder diffraction were quartz and braunite. Phase enrichment of pumpellyite in the powder specimens was performed by granulometric fractionation, separation by heavy liquids, and magnetic separation (Frantz Isodynamic Magnetic Separator). The best results were obtained by magnetic separation of the fractions with grain size <0.063 mm, using currents in the range 0.55–0.65 Amp and transverse and longitudinal slopes of 18 and 30°, respectively. Quartz and braunite impurities were removed below the limits of detection by X-ray diffraction, although by careful check of the powder spectra, a few residual powder diffraction lines (at d = 4.75, 4.38, and 3.03 Å) were interpreted as an indication of the presence of orientite. This mineral species has not been found associated with pumpellyite to date, although its structural relationship to other Mn-rich silicates such as macfallite, sursassite, and ardennite (Moore et al. 1979, 1985; Mellini et al. 1986), all of which are known to present intergrowth and polytypic relationship with pumpellyite (Allmann and Donnay 1971; Mellini et al. 1984; Pasero and Reinecke 1991), makes the orientite-pumpellyite association plausible.

Electron probe microanalyses were performed on several polycrystalline grains from each sample. The analyses showed that a certain degree of chemical inhomogeneity is present between different grains and between different spot analyses performed on the same particle. This chemical inhomogeneity is frequently found in pumpellyite, and it is caused by the small size of the fibrous pumpellyite crystals, the presence of voids in the fiber bundles, the presence of other mineral microimpurities, and of course by true chemical variability in the crystals. The mean chemical analyses and the observed range for both pumpellyite samples are reported in Table 1. The average chemical formulas were calculated assuming a fixed weight loss of H_2O (7.0 wt%; this value is the average weight loss of pumpellyite samples from different localities; see Deer et al. 1985) and assuming all Fe as Fe_2O_3 and all Mn as MnO.

The number of Mn atoms per unit cell obtained for the two pumpellyite samples, SN1 and SN5, is 3.41 and 1.85, respectively. The change in total Mn content is negligible if the stoichiometric formulas are recalculated assuming all Fe as FeO or a different Mn_2O_3/MnO ratio, and the unit formulas can be approximated as SN1 = $Ca_{8.12}(Al_{7.99}Mn_{3.41}Mg_{0.71}Fe_{0.30})Si_{11.84}O_{56-x}OH_x$ and SN5 = $Ca_{7.80}(Al_{8.91}Mn_{1.85}Mg_{1.16}Fe_{0.37})Si_{11.92}O_{56-x}OH_x$. The two samples are representative of known occurrences of Mn-rich pumpellyite minerals of metamorphic origin, although hydrothermal pumpellyite minerals have been reported with higher Mn contents (Dasgupta et al. 1991).

Collection of powder X-ray diffraction data and Rietveld structure refinement

The X-ray powder spectra of the two pumpellyite specimens were measured at different wavelengths in proximity to and far from the MnK absorption edge, using synchrotron radiation in the high-resolution angle-scanning mode at the Synchrotron Radiation Source (SRS), Daresbury Laboratory, U.K., at beam line 2.3. The X-ray absorption spectrum of a reference compound containing Mn in both valence states (synthetic hausmannite, $Mn^{2+}Mn_2^{3+}O_4$) was measured first to calibrate the energy position of the absorption edge. The absorption scan and its first derivative are shown in Figure 1. The position of the MnK edge was taken as the maximum of the first derivative curve (λ = 1.8901 Å) corresponding to an energy of 6561 eV, in comparison with an ideal binding energy for neutral Mn of 6539 eV (Williams 1986). Powder spectra were then measured for pumpellyite samples SN1 and SN5 and for the reference spinel compound Mn_3O_4 at about 20, 50, and 200 eV above the absorption edge. A Ge(111) monochromator (d_{111} = 3.26627 Å) was used to select the wavelengths for data collections, and the experimental setup encompassed a flat-sample par-

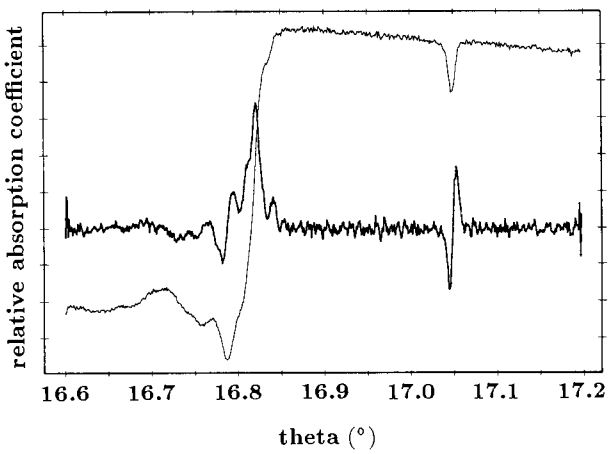

FIGURE 1. Energy scan at the position of the Mn K absorption edge for synthetic hausmannite. The thin line is the plot of the normalized absorption coefficient, and the thick line is the first derivative of the absorption curve. The vertical axis represents the normalized absorption values in arbitrary units, and the horizontal axis represents the θ angle of the Ge(111) monochromator in degrees. The maximum of the first derivative curve at θ = 16.818° corresponds to an energy of 6561 eV.

allel-beam geometry, with primary slits of 1.3 × 10.0 mm and long soller receiving slits. Data were collected in the angular range 20–120° 2θ, with scan steps of 0.01° 2θ and counting times of 2 s/step.

The off-edge powder scan of pumpellyite sample SN5 was corrupted because of vacuum problems, and therefore it was decided to collect two supplementary powder spectra with conventional instrumentation, so as to have at least one full data set unaffected by resonant scattering for each sample. The addition of data collected far from the absorption edge greatly helped in the convergence of the Rietveld multispectra refinement toward a stable minimum, in the correct determination of the atomic displacement parameters, and in reducing the correlation between atomic displacement parameters, site-occupancy factors, and site-resolved anomalous scattering coefficients. These spectra also provided a reference wavelength for the refinement of the cell parameters, and therefore allowed unbiased refinement of the wavelength in the synchrotron radiation data sets.

The two conventional powder diffraction data sets were collected in Bragg-Brentano geometry on a Philips instrument using Cu$K\alpha$ radiation, a diffracted-beam graphite monochromator, step scans of 0.02° 2θ, counting times of 15 s/step, and the angular ranges 17.8–105.8 (sample SN1) and 17.8–127.2° (sample SN5). Details of the data-collection parameters and the refined wavelengths for the synchrotron spectra are reported in Table 2.

The powder data were used in a multispectra Rietveld refinement with the GSAS software (Larson and Von Dreele 1995). A unique structure model for each sample was refined at the same time against all available data sets. The least-squares minimization therefore included structure-dependent parameters (lattice constants, atomic coordinates, site occupancies, isotropic atomic displacement parameters) and histogram-dependent parameters (wavelength, zero 2θ shift, coefficients of the peak-profile function, coefficients of the background-profile function, scale factor, preferred orientation correction, anomalous-scattering coefficients). Starting atomic coordinates were from Yoshiasa and Matsumoto (1985). A pseudo-Voigt function corrected for asymmetry was used to model the diffraction-peak profiles, and the background was modeled using a cosine Fourier series with six coefficients. A preferred orientation correction was applied because the fibrous morphology of the pumpellyite crystals is known to affect the diffraction spectra strongly (Artioli and Geiger 1994). The preferred orientation effect was treated by applying both a correction coefficient on the [010] zone axis following the March-Dollase formulation (Dollase 1986) and an anisotropic broadening parameter along [010] included in the Lorentzian part of the pseudo-Voigt function and corresponding to the Scherrer broadening effect.

TABLE 2. Unit-cell dimensions and Mn site contents of pumpellyite and data collection parameters

	Sample SN1	Sample SN5
Cell a (Å)	8.8510(3)	8.8330(4)
b (Å)	5.9345(2)	5.9153(3)
c (Å)	19.1247(6)	19.1009(8)
β (°)	96.969(1)	97.154(2)
Mn(X) (mult. 4)	1.31(3)	1.07(4)
Mn(Y) (mult. 8)	2.10(3)	0.83(3)
	Powder spectrum 1	
npts	10001	10001
2θ range (°)	20–120	20–120
Wavelength (Å)	1.89649(6)	1.9021(1)
R_p	0.0962	0.0955
R_{wp}	0.1235	0.1210
Mn f'(X)	−7.2(4)	−5.8(4)
Mn f'(Y)	−5.5(3)	−5.2(6)
	Powder spectrum 2	
npts	9184	10001
2θ range (°)	20–111.8	20–120
Wavelength (Å)	1.90841(6)	1.9088(1)
R_p	0.1077	0.0930
R_{wp}	0.1379	0.1189
Mn f'(X)	−4.8(4)	−5.0(4)
Mn f'(Y)	−4.6(3)	−4.5(6)
	Powder spectrum 3	
npts	10001	
2θ range (°)	20–120	
Wavelength (Å)	1.94148(7)	
R_p	0.1080	
R_{wp}	0.1378	
Mn f'(X)	−3.51	
Mn f'(Y)	−3.51	
	Powder spectrum 4	
npts	4401	5471
2θ range (°)	17.8–105.8	17.8–127.2
Wavelength (Å)	Cu$K\alpha$	Cu$K\alpha$
R_p	0.1054	0.1066
R_{wp}	0.1356	0.1345
Mn f'(X)	−0.57	−0.57
Mn f'(Y)	−0.57	−0.57

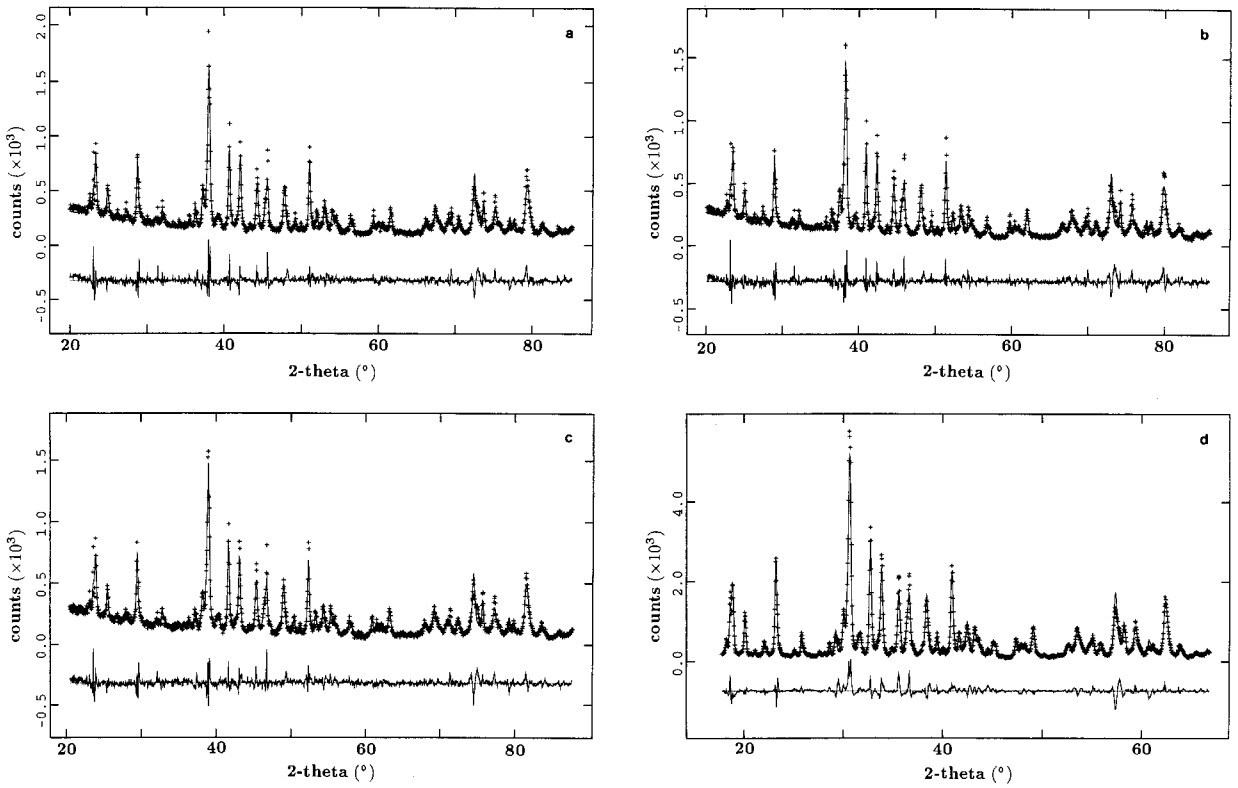

FIGURE 2. Observed, calculated, and difference final profiles for the Rietveld refinement of pumpellyite sample SN1. The data sets were collected at the following wavelengths: (**a**) 1.89654(6) Å, (**b**) 1.90841(6) Å, (**c**) 1.94148(7) Å, and (**d**) Cu$K\alpha$ radiation. Each powder profile is shown in the angular range corresponding to d values in the range 1.40–5.46 Å.

Independent f' site-resolved anomalous scattering coefficients were refined for the X and Y octahedral Mn cations for the synchrotron data collected in proximity of the MnK absorption edge. The f'' coefficients were fixed at the ideal values calculated with a modified version of the FPRIME program (Cromer 1965) for the off-edge synchrotron data and for the conventional data.

Because of the complexity of the refinement, several crystal-chemical and crystallographic constraints were imposed to improve convergence: (1) Mg determined from the electron probe microanalysis was assumed to occupy exclusively the X octahedral site and was fixed in the refinement. (2) Full occupancy of the X and Y octahedral sites was assumed: Al(X) + Mn(X) + Mg(X) = 1.0 and Al(Y) + Mn(Y) = 1.0. The Fe content in both sites was neglected, as in the worst case Fe(X + Y) is about 3% of the octahedral site occupancy. The slight underestimation of the site-scattering density is assumed to induce only a small bias in the refined atomic displacement parameters. (3) The sum of Mn(X) + Mn(Y) for each sample was constrained to the mean total Mn content determined by electron probe microanalysis. (4) Isotropic atomic displacement parameters (a.d.p.) were refined in groups according to chemical species. Four a.d.p. were refined in each structure: one for the tetrahedral Si atoms, one for the O,OH atoms, one for the Ca atoms, and one for the octahedral atoms. The X and Y octahedral sites were constrained to have equal a.d.p. values to avoid correlation with the Mn intersite distribution. (5) The diffraction-profile function of the synchrotron powder spectra was assumed to be wavelength independent, and therefore a unique set of coefficients of the pseudo-Voigt function was refined for all the synchrotron diffraction spectra pertaining to the same sample. (6) Soft constraints on Si-O and O-O distances were imposed in the early stages of the refinement and gradually released in the final stages. The bond constraints were treated as additional observables during the least-squares minimization. (7) The coefficient of the preferred orientation correction was constrained to be equal for the synchrotron histograms of each sample because the powder specimen was mechanically packed in the sample holder at the start of the experiment and left untouched during the data collection at different wavelengths. This constraint is not strictly valid, however, because different wavelengths have different penetration depths. This constraint was applied to reduce the number of variables in the refinement. Furthermore, the attempted refinement of a separate correction param-

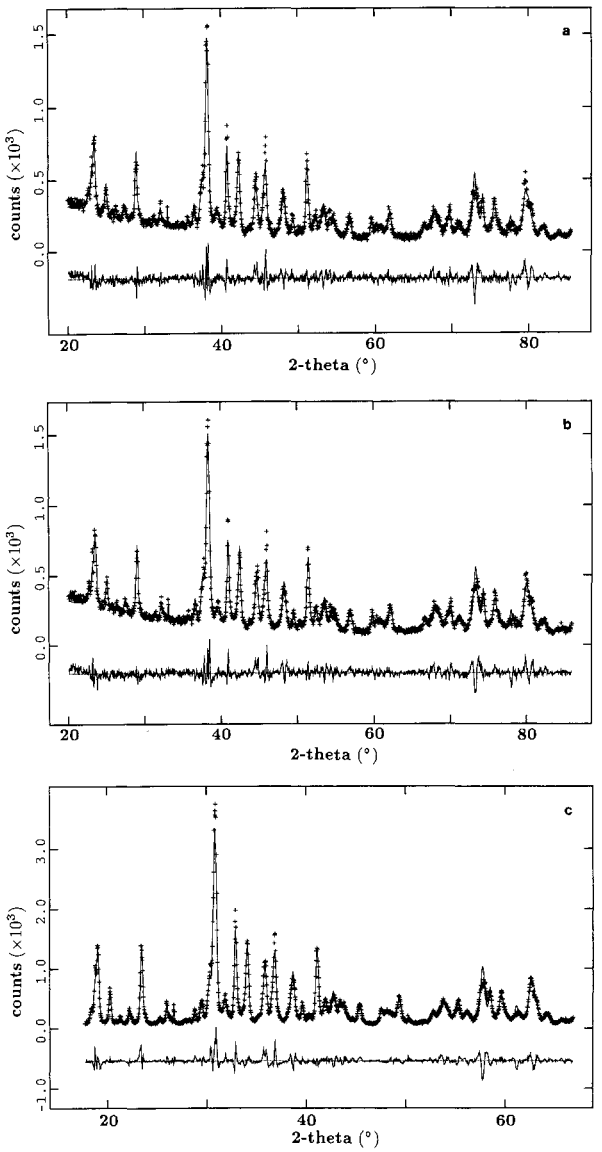

FIGURE 3. Observed, calculated, and difference final profiles for the Rietveld refinement of pumpellyite sample SN5. The data sets were collected at the following wavelengths: (a) 1.9021(1) Å, (b) 1.9088(1) Å, and (c) Cu$K\alpha$ radiation. Each powder profile is shown in the angular range corresponding to d values in the range 1.40–5.46 Å.

TABLE 3. Refined atomic coordinates and isotropic displacement parameters of pumpellyite

Atom	x	y	z	U_{iso}
		Sample SN1		
Si1	0.0453(5)	0.0	0.0896(2)	0.0269(6)
Si2	0.1670(4)	0.0	0.2493(2)	0.0269(6)
Si3	0.4529(4)	0.0	0.4011(2)	0.0269(6)
X*	½	¼	¼	0.0346(6)
Y*	0.2530(4)	0.2475(7)	0.4954(2)	0.0346(6)
Ca1	0.2529(3)	½	0.3387(1)	0.0190(6)
Ca2	0.1943(3)	½	0.1554(2)	0.0190(6)
O1	0.1332(5)	0.2358(6)	0.0742(2)	0.0126(5)
O2	0.2733(5)	0.2252(5)	0.2522(3)	0.0126(5)
O3	0.3592(5)	0.2331(6)	0.4142(2)	0.0126(5)
O4	0.1300(6)	½	0.4456(3)	0.0126(5)
OH5	0.1268(7)	0.0	0.4583(4)	0.0126(5)
O6	0.3815(6)	½	0.0495(3)	0.0126(5)
OH7	0.3714(7)	0.0	0.0348(4)	0.0126(5)
O8	0.0465(6)	0.0	0.1772(2)	0.0126(5)
O9	0.4723(7)	½	0.1753(3)	0.0126(5)
OH10	0.0679(7)	0.0	0.3171(3)	0.0126(5)
OH11	0.5113(7)	½	0.3155(4)	0.0126(5)
		Sample SN5		
Si1	0.0428(5)	0.0	0.0896(2)	0.0245(7)
Si2	0.1649(4)	0.0	0.2490(2)	0.0245(7)
Si3	0.4612(5)	0.0	0.4018(2)	0.0245(7)
X*	½	¼	¼	0.0305(8)
Y*	0.2478(5)	0.2483(8)	0.4950(2)	0.0305(8)
Ca1	0.2527(3)	½	0.3388(2)	0.0245(8)
Ca2	0.1925(3)	½	0.1548(2)	0.0245(8)
O1	0.1360(5)	0.2296(7)	0.0714(3)	0.0107(6)
O2	0.2703(6)	0.2264(6)	0.2496(3)	0.0107(6)
O3	0.3608(5)	0.2268(7)	0.4154(3)	0.0107(6)
O4	0.1349(6)	½	0.4460(4)	0.0107(6)
OH5	0.1283(8)	0.0	0.4575(4)	0.0107(6)
O6	0.3743(6)	½	0.0477(4)	0.0107(6)
OH7	0.3753(8)	0.0	0.0320(4)	0.0107(6)
O8	0.0439(7)	0.0	0.1767(2)	0.0107(6)
O9	0.4761(7)	½	0.1768(3)	0.0107(6)
OH10	0.0677(7)	0.0	0.3173(3)	0.0107(6)
OH11	0.5045(8)	½	0.3155(4)	0.0107(6)

* Occupancy factors of the octahedral cation sites are as follows: For SN1, X = $Mg_{0.178}$, $Al_{0.494}$, $Mn_{0.328}$, Y = $Al_{0.738}$, $Mn_{0.262}$; and for SN5, X = $Mg_{0.290}$, $Al_{0.442}$, $Mn_{0.288}$, Y = $Al_{0.897}$, $Mn_{0.103}$.

eter for each histogram resulted in coefficients indicating a similar, moderate preferred orientation effect in all the powder profiles.

A total of four powder diffraction spectra (33622 step intensities) and 95 variables were refined simultaneously for pumpellyite sample SN1, and a total of three powder diffraction spectra (25510 step intensities) and 89 variables were refined for sample SN5. Final agreement factors for the total data sets are R_{wp} = 0.133, R_p = 0.104, and R_{F^2} = 0.091 for sample SN1, and R_{wp} = 0.125, R_p = 0.098, and R_{F^2} = 0.114 for sample SN5. Observed, calculated, and difference powder diffraction spectra for samples SN1 and SN5 are shown in Figures 2 and 3, respectively.

Final atomic coordinates and isotropic displacement parameters for the two samples are listed in Table 3. Selected interatomic distances and angles are reported in Table 4.

RESULTS AND DISCUSSION

The simultaneous refinement of several powder spectra using resonant X-ray diffraction data is a powerful tool for determining the cation site distribution within disordered materials (e.g., Attfield 1990; Kwei et al. 1990; Perkins and Attfield 1991; Wilkinson et al. 1992), and in principle the site occupancy of every element for which resonant scattering data are available can be treated as an

TABLE 4. Selected interatomic distances (Å) and angles (°) for the coordination polyhedra in pumpellyite

	Sample SN1	Sample SN5
Si1-O1 × 2	1.645(3)	1.648(3)
Si1-O4	1.614(4)	1.631(4)
Si1-O8	1.674(4)	1.661(4)
Si2-O2 × 2	1.631(3)	1.630(3)
Si2-O8	1.638(4)	1.639(4)
Si2-OH10	1.651(4)	1.649(4)
Si3-O3 × 2	1.648(3)	1.646(3)
Si3-O6	1.645(2)	1.641(4)
Si3-O9	1.675(2)	1.664(4)
X-O2 × 2	2.018(4)	2.033(5)
X-O9 × 2	2.054(4)	2.028(4)
X-OH11 × 2	1.936(4)	1.934(5)
Y-O1	1.946(5)	1.866(6)
Y-O3	1.914(5)	1.925(5)
Y-O4	2.022(5)	1.964(6)
Y-OH5	1.928(5)	1.897(6)
Y-O6	2.058(5)	2.034(5)
Y-OH7	1.929(5)	1.945(6)
Ca1-O2 × 2	2.345(5)	2.369(5)
Ca1-O3 × 2	2.269(4)	2.305(5)
Ca1-O4	2.430(7)	2.410(8)
Ca1-O8	2.630(6)	2.599(6)
Ca1-OH11	2.382(6)	2.322(7)
Ca2-O1 × 2	2.227(5)	2.269(5)
Ca2-O2 × 2	2.503(5)	2.461(5)
Ca2-O6	2.768(7)	2.753(8)
Ca2-O9	2.444(6)	2.488(7)
Ca2-OH10	2.441(6)	2.422(6)
O1-Si1-O1	116.6(4)	111.0(5)
O1-Si1-O4 × 2	112.2(2)	113.1(3)
O1-Si1-O8 × 2	103.5(3)	105.7(3)
O4-Si1-O8	107.8(4)	107.6(4)
O2-Si2-O2	110.0(4)	110.5(4)
O2-Si2-O8 × 2	110.1(3)	108.5(3)
O2-Si2-OH10 × 2	109.4(3)	110.4(3)
O8-Si2-OH10	107.9(4)	108.5(4)
O3-Si3-O3	114.2(4)	109.2(4)
O3-Si3-O6 × 2	110.1(2)	111.3(3)
O3-Si3-O9 × 2	113.1(2)	112.9(3)
O6-Si3-O9	94.7(4)	99.2(4)

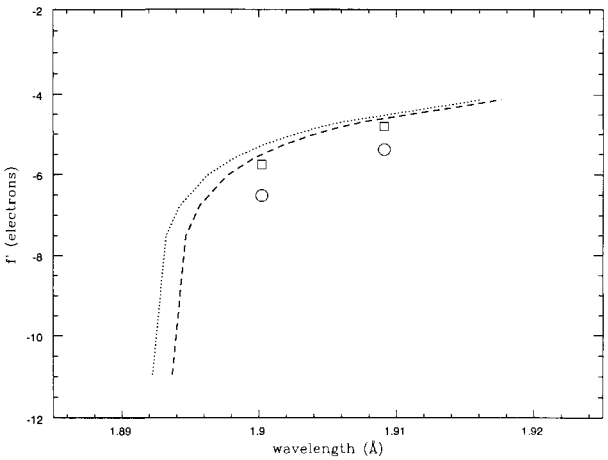

FIGURE 4. Theoretical curves for the values of the f' anomalous scattering coefficient in proximity of the Mn K absorption edge. The values were calculated with the FPRIME program (Cromer 1965) for an isolated neutral Mn atom and then shifted to higher energies by the chemical shift observed in the literature by XANES spectroscopy for divalent (dashed line) and trivalent (dotted line) Mn ions. Open squares and circles refer to the refined f' values for Mn in the octahedral and tetrahedral sites, respectively, of synthetic hausmannite (Mn_3O_4). Error bars are not shown because they are much smaller than the plotted symbols.

independent variable in the case of multiple site occupancy (Aranda et al. 1994). The method has also been employed to resolve valence ambiguities between cation sites when different oxidation states of the element of interest are partitioned over distinct crystallographic sites (e.g., Wilkinson et al. 1991; Warner et al. 1992; Wilkinson and Cheetham 1992; Gao et al. 1992).

To illustrate the principles of the method and what one should expect from the refinement of the anomalous scattering coefficients, in Figure 4 we report the theoretical curve of the energy dependence of the f' coefficient for neutral Mn computed with FPRIME. The same curve is shifted in energy by an amount experimentally determined by XANES for the chemical shift of Mn^{2+} and Mn^{3+} (Brown et al. 1988; Kohn et al. 1990). This corresponds to shifts of 6 eV between Mn^{2+} and neutral Mn, and 4 eV between Mn^{3+} and Mn^{2+}.

It can be seen that at all wavelengths above the absorption edge the f' anomalous dispersion coefficient of Mn^{2+} is always much smaller than the f' value of Mn^{3+}. The difference becomes vanishingly small far from the absorption edge. For comparison, in Figure 4 we show the refined f' coefficients for the standard Mn_3O_4 compound at two wavelengths below the absorption edge [1.900217(4) and 1.909083(4) Å]. Hausmannite has the normal spinel structure, with complete partitioning of Mn^{2+} in the tetrahedral site and Mn^{3+} in the octahedral site. The results are in perfect agreement with the prediction that f' values for Mn^{2+} are noticeably smaller than the f' values for Mn^{3+} at both wavelengths. The observed points are also in good qualitative agreement with the shape of the theoretical curves, although the difference between the experimental points at each wavelength is larger than the difference expected between the theoretical values. This "amplification" of the resonance effect, which can also be interpreted as a larger chemical shift of the absorption edge in relation to the difference in the oxidation state, has been observed before and is generally ascribed to the fact that the theoretical calculations for the free atom do not consider the near-edge oscillations from the EXAFS. It is therefore expected that the true shapes of the Mn^{2+} and Mn^{3+} curves strongly deviate from those of the theoretical curves because of the chemical environment of the bonded Mn cations in the structure (Cox and Wilkinson 1994).

The energy band pass of the incident radiation due to the Darwin width of the Ge(111) monochromator is about 3 eV, including divergence effects, with a corresponding wavelength spread of about 0.001 Å. Although the band pass is substantially greater than the natural width of the absorption edge, we estimated that the effect is important only at wavelengths extremely close to the absorption

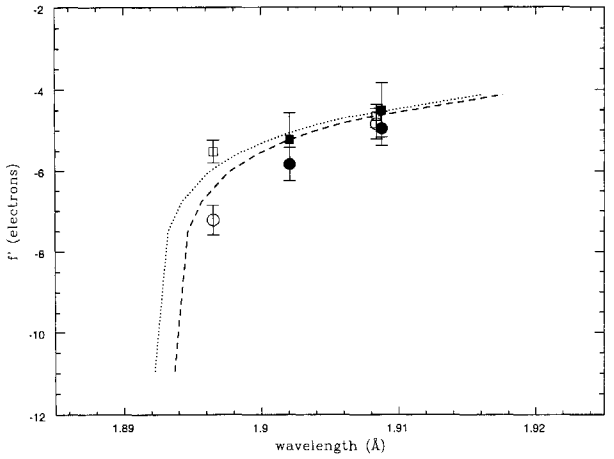

FIGURE 5. Refined f' anomalous scattering coefficients for Mn in the octahedrally coordinated sites of pumpellyite samples SN1 (open symbols) and SN5 (solid symbols). Circles and squares refer to the X and Y octahedral sites, respectively. The dashed and dotted curves were drawn as reference lines and have the same meaning as in Figure 4.

edge, and that it is negligible for data collected more than 50 eV above it. Furthermore, even at wavelengths in close proximity to the absorption edge, the energy spread mainly influences the sharper discontinuity in the f'' curve rather that the broader changes in the f' curve. We did not consider refining the f'' coefficients in the present work because the magnitude of the resonant scattering effect of the imaginary part of the dispersion correction is much smaller than that of the real part, especially in centrosymmetric structures.

There is, however, no doubt that the resonant scattering powder data contain sufficient information in the energy region explored in the present experiments to allow proper discrimination between the two oxidation states of Mn in the hausmannite structure.

The refined f' coefficients for the X and Y sites in pumpellyite samples SN1 and SN5 are plotted in Figure 5. In the off-edge data set the f' values were fixed at the theoretical values calculated with FPRIME for both sites ($f' = -3.51$ e for the data set collected at 1.94148 Å; $f' = -0.57$ e for the data sets collected with Cu$K\alpha$ radiation), so as to have absolute f' values closer to the theoretical curves and to minimize correlation with the Mn content of the sites.

It is evident that for all data sets collected near the K absorption edge the refined Mn f' value of the X octahedral site is smaller than the refined value for the Y octahedral site. The observed difference is systematic: It decreases in magnitude from the data sets close to the K edge [1.8965 Å: $f'(Y) - f'(X) = 1.7$ e; 1.9021 Å: $f'(Y) - f'(X) = 0.6$ e] to the data sets removed from the edge [1.9084 Å: $f'(Y) - f'(X) = 0.2$ e; 1.9088 Å: $f'(Y) - f'(X) = 0.4$ e], and it is independent of the refined Mn content of the site.

We therefore interpret the results as a clear indication that the Mn cations in pumpellyite are partitioned in the two octahedral sites, and that the larger site X is essentially occupied by Mn^{2+}, whereas the smaller site Y is occupied by Mn^{3+} cations. This interpretation is consistent with the ionic size difference between the two octahedrally coordinated cations (Mn^{2+} ionic radius = 0.830 Å; Mn^{3+} ionic radius = 0.645 Å; Shannon 1976) and with the observed partitioning of Fe^{2+} and Fe^{3+} in Fe-rich pumpellyite minerals (Artioli and Geiger 1994).

CONCLUSIONS

X-ray powder diffraction data taking advantage of the resonant scattering effect were collected in proximity of the Mn absorption K edge on two Mn-rich pumpellyite samples from the East Ligurian Apennines. The results of a multispectral Rietveld refinement clearly indicate that the Mn cations are distributed over the two octahedrally coordinated structural sites, and that the Mn^{2+} and Mn^{3+} cations are partitioned in the X and Y octahedral sites, respectively. This interpretation is in agreement with the assumption that site Y accommodates only trivalent cations in all known pumpellyite compositions in the pumpellyite-julgoldite-okhotskite field (Dasgupta et al. 1991). However, because of the varying number of OH groups in the structure and the simultaneous presence of the divalent oxidation state of the same transition elements in the X site, it is virtually impossible to predict the distribution of the transition elements (mainly Mn and Fe) in the octahedral structural sites, and therefore the divalent/trivalent ratio of the elements, on the basis of the bulk-chemical analysis. A detailed structure analysis by spectroscopic or diffraction methods is required to determine properly the correct oxidation state of the mixed valence cations in pumpellyite-group minerals.

ACKNOWLEDGMENTS

This research has been supported by MURST and CNR funds to G.A. Synchrotron experiments were made possible by CEE funds to Daresbury Laboratory under the Large Installation Plan. Bob Von Dreele and Angus Wilkinson are thanked for constructive reviews.

REFERENCES CITED

Allmann, R., and Donnay, G. (1971) Structural relations between pumpellyite and ardennite. Acta Crystallographica, B27, 1871–1875.

——— (1973) The crystal structure of julgoldite. Mineralogical Magazine, 39, 271–281.

Aranda, M.A.G., Sinclair, D.C., and Attfield, J.P. (1994) Cation distribution in the superconducting Tl, Pb-1223 phase ("$Tl_{0.5}Pb_{0.5}Sr_2Ca_2Cu_3O_9$") from resonant synchrotron powder X-ray diffraction. Physica C, 221, 304–310.

Artioli, G. (1980) Ricerche strutturali sulla pumpellyite, minerale epimetamorfico, 98 p. Tesi di Laurea, Istituto di Mineralogia e Petrologia, Universita di Modena, Modena, Italy.

Artioli, G., Sacchi, M., Balerna, A., Burattini, E., and Simeoni, S. (1991) XANES studies of Fe in pumpellyite-group minerals. Neues Jahrbuch für Mineralogie Monatshefte, 9, 413–421.

Artioli, G., and Geiger, C.A. (1994) The crystal chemistry of pumpellyite: An X-ray Rietveld refinement and ^{57}Fe Mössbauer study. Physics and Chemistry of Minerals, 20, 443–453.

Artioli, G., Quartieri, S., and Deriu, A. (1995) Spectroscopic data on

coexisting prehnite-pumpellyite and epidote-pumpellyite. Canadian Mineralogist, 33, 67–75.

Attfield, J.P. (1990) Determination of valence and cation distributions by resonant powder X-ray diffraction. Nature, 343, 46–49.

Baur, W.H. (1971) The prediction of bond length variations in silicon-oxygen bonds. American Mineralogist, 56, 1573–1599.

Brown, G.E., Calas, G., Waychunas, G.A., and Petiau, J. (1988) X-ray absorption spectroscopy: Applications in mineralogy and geochemistry. In Mineralogical Society of America Reviews in Mineralogy, 18, 431–512.

Cortesogno, L., Lucchetti, G., and Spadea, P. (1984) Pumpellyite in low-grade metamorphic rocks from Ligurian and Lucanian Apennines, Maritime Alps, and Calabria (Italy). Contributions to Mineralogy and Petrology, 85, 14–24.

Cox, D.E., and Wilkinson, A.P. (1994) Resonant anomalous X-ray scattering theory and applications, 450 p. North-Holland, Amsterdam.

Cromer, D.L. (1965) Anomalous dispersion corrections computed from self-consistent field relativistic Dirac-Slater wave functions. Acta Crystallographica, 18, 17–23.

Dasgupta, S., Chakraborti, S., Sengupta, P., Bhattacharya, P.K., Banerjee, H., Roy, S., and Fukuoka, M. (1991) Manganese-rich minerals of the pumpellyite group from the Precambrian Sausar Group, India. American Mineralogist, 76, 241–245.

Deer, W.A., Howie, R.A., and Zussmann, J. (1985) Rock forming minerals, vol. 1B: Disilicates and ring silicates (2nd edition) p. 201–247. Longman, Harlow, U.K.

Dollase, W.A. (1986) Correction of intensities for preferred orientation in powder diffractometry: Application of the March model. Journal of Applied Crystallography, 19, 267–272.

Frey, M., De Capitani, C., and Liou, J.G. (1991) A new petrogenetic grid for low-grade metabasites. Journal of Metamorphic Geology, 9, 497–509.

Galli, E., and Alberti, A. (1969) On the crystal structure of pumpellyite. Acta Crystallographica, B25, 2276–2281.

Gao, Y., Frost-Jensen, A., Pressprich, M.R., and Coppens, P. (1992) Valence contrast by synchrotron resonance scattering: Applications to a mixed valence Mn compound. Journal of the American Chemical Society, 114, 9214–9215.

Gottardi, G. (1965) Die Kristallstruktur von Pumpellyit. Tschermaks Mineralogische und Petrograpische Mitteilungen, 10, 115–119.

Ivanov, O.K., Arkhangel'skaya, V.A., Miroshnikova, L.O., and Shilova, T.A. (1981) Shuiskite, the chromium analogue of pumpellyite, from the Bisersk deposit. Zapiski Vsesoyuznogo Mineralogicheskogo Obshchestva, 110, 508–512.

Kato, A., Matsubara, S., and Yamamamoto, R. (1981) Pumpellyite-(Mn^{2+}) from the Ochiai Mine, Yamanashi Prefecture, Japan. Bulletin de Minéralogie, 104, 396–399.

Kohn, S.C., Charnock, J.M., Henderson, C.M.B., and Greaves, G.N. (1990) The structural environment of trace elements in dry and hydrous silicate glasses: A manganese and strontium *K*-edge X-ray absorption spectroscopic study. Contributions to Mineralogy and Petrology, 105, 359–368.

Kwei, G.H., Von Dreele, R.B., Cheong, S.-W., Fisk, Z., and Thompson, J.D. (1990) Structure of T^*-phase superconductors: Anomalous X-ray diffraction study of cation ordering in $La_{0.9}Gd_{0.9}Sr_{0.2}CuO_4$. Physical Review B, 41, 1889–1893.

Larson, A.C., and Von Dreele, R.B. (1995) GSAS General Structure Analysis System. Document LAUR 86-748, Los Alamos National Laboratory, Los Alamos, New Mexico.

Lucchetti, G. (1983) Mn-rich pumpellyite from Eastern Liguria (Italy). Neues Jahrbuch für Mineralogie Monatshefte, 12, 563–568.

Mellini, M., Merlino, S., and Pasero, M. (1984) X-ray and HRTEM study of sursassite: Crystal structure, stacking disorder, and sursassite-pumpellyite intergrowth. Physics and Chemistry of Minerals, 10, 99–105.

——— (1986) X-ray and HRTEM structure analysis of orientite. American Mineralogist, 71, 176–187.

Moore, P.B. (1971) Julgoldite, the Fe^{2+}-Fe^{3+} dominant pumpellyite. Lithos, 4, 93–99.

Moore, P.B., Ito, J., and Steele, I.M. (1979) MacFallite and orientite: Calcium manganese (III) silicates from upper Michigan. Mineralogical Magazine, 43, 325–331.

Moore, P.B., Shen, J., and Araki, T. (1985) Crystal chemistry of the $^{2}_{\infty}[M^{3+}_{2}\phi_2(TO_4)_2]$ sheet: Structural principles and crystal structures of ruizite, macfallite and orientite. American Mineralogist, 70, 171–181.

Pan, Y., and Fleet, M.E. (1992) Vanadium-rich minerals of the pumpellyite group from the Hemlo gold deposit, Ontario. Canadian Mineralogist, 30, 153–162.

Pasero, M., and Reinecke, T. (1991) Crystal chemistry, HRTEM analysis and polytypic behaviour of ardennite. European Journal of Mineralogy, 3, 819–830.

Passaglia, E., and Gottardi, G. (1973) Crystal chemistry and nomenclature of pumpellyites and julgoldites. Canadian Mineralogist, 12, 219–223.

Perkins, D.A., and Attfield, J.P. (1991) Resonant powder X-ray determination of the cation distribution in $FeNi_2BO_5$. Journal of the Chemical Society, Chemical Communications, 229–231.

Shannon, R.D. (1976) Revised effective ionic radii and systematic studies of interatomic distances in halides and chalcogenides. Acta Crystallographica, A32, 751–767.

Togari, K., and Akasaka, M. (1987) Okhotskite, a new mineral, an Mn^{3+}-dominant member of the pumpellyite group, from the Kokuriki mine, Hokkaido, Japan. Mineralogical Magazine, 51, 611–614.

Warner, J.K., Cheetham, A.K., Cox, D.E., and Von Dreele, R.B. (1992) Valence contrast between iron sites in α-Fe_2PO_5: A comparative study by magnetic neutron and resonant X-ray powder diffraction. Journal of the American Chemical Society, 114, 6074–6080.

Wilkinson, A.P., Cheetham, A.K., and Cox, D.E. (1991) Study of oxidation-state contrast in gallium dichloride by synchrotron X-ray anomalous scattering. Acta Crystallographica, B47, 155–161.

Wilkinson, A.P., and Cheetham, A.K. (1992) Valence-contrast studies by resonant diffraction with synchrotron radiation: The role of X-ray absorption measurements. Journal of Applied Crystallography, 25, 654–657.

Wilkinson, A.P., Cheetham, A.K., Tang, S.C., and Repport, W.J. (1992) Cation distribution in zeolites Zn/Na-Y by resonant X-ray diffraction. Journal of the Chemical Society, Chemical Communications, 1485–1487.

Williams, G.P. (1986) Electron binding energies for the elements. In D. Vaughan, Ed., X-ray data booklet, section 2.2, Lawrence Berkeley Laboratory Pub. 490.

Yoshiasa, A., and Matsumoto, T. (1985) Crystal structure refinement and crystal chemistry of pumpellyite. American Mineralogist, 70, 1011–1019.

Manuscript received June 1, 1995
Manuscript accepted January 17, 1996